Seasonal and Low-Frequency Variability of the Meridional Heat Flux at 36°N in the North Atlantic

OLGA T. SATO

Jet Propulsion Laboratory, California Institute of Technology, Pasadena, California

T. ROSSBY

Graduate School of Oceanography, University of Rhode Island, Kingston, Rhode Island

ABSTRACT

Historical hydrographic sections are used to investigate the seasonal and interannual variability in the meridional heat flux at 36°N in the North Atlantic. The data consist of ten transatlantic sections and sections from four sectors, which combined, cross the entire basin. These sectors are the slope water, the Gulf Stream, the Sargasso Sea, and the midocean. The data from the first three sectors actually come from sections that span all three regions, but their properties are examined individually. To improve estimates of the Gulf Stream contribution to the total heat flux, a tangent hyperbolic model of the current's temperature field is used to retain its structure in the temperature flux integrations even when only a few stations are available. The technique removes biases due to undersampling that averages about 0.3 PW.

The temperature flux of the upper layer is estimated for the four sectors plus the climatologically forced Ekman layer. The annual mean is 1.4 ± 0.3 PW with a range of 0.6 ± 0.1 PW. The zero net mass flux across the transect can be accomplished by assuming that in the deep layer an equivalent amount of water to that estimated for the upper layer flows in the southward direction presumably via the deep western boundary current. The temperature flux of the deep layer, with its mean temperature of 2.3°C, has an annual mean of −0.20 ± 0.06 PW and a range of 0.05 ± 0.02 PW. The net annual mean of the meridional heat flux is 1.2 ± 0.3 PW and a range of 0.6 ± 0.1 PW. Its phase is dominated by the annual cycle of the Ekman temperature flux.

The heat flux residual is examined for evidence of long-term change in the poleward heat flux. While the database is very limited for a conclusive statement, it appears that the residual for the pentads 1935–39, 1970–74, and 1975–79 agreed to within 0.1 PW. The tightness of these estimates in the presence of a 0.6 PW annual range makes it clear how important it is to know the latter accurately before statements about long-term change can be made. To date, most individual transoceanic sections were taken during the summer and spring. The standard deviation of the heat flux estimates is 0.3 PW, much of it due to eddy variability, making it essential to obtain repeat sections preferably with a uniform distribution throughout the year.

1. Introduction

The oceans play a central role in maintaining the patterns of global climate, via its enormous heat capacity and because of the redistribution of incoming heat by the wind-driven and thermohaline forcing of the ocean currents. Thus, the surplus of heat at low latitudes is redirected toward higher latitudes by the oceans (and atmosphere) to maintain the global temperature distribution as we know it. In the oceans, the fast-flowing western boundary currents play a major role in facilitating the meridional redistribution of heat and thereby maximizing the temperature meridional gradient around the midlatitudes. The interest of the scientific community in understanding and correctly modeling the global climate requires accurate knowledge of the meridional transport of heat variability.

Several studies investigated the heat transport variability in the North Atlantic. Rago and Rossby (1987) used hydrographic sections, current meters, and direct velocity measurements from Pegasus velocity profiler to obtain an annual mean and seasonal variability of the heat flux at 32°N. Molinari et al. (1990) used Levitus (1982) climatological data in the interior of the ocean with the direct velocity and temperature measured in the Florida Straits to estimate the heat flux at 26.5°N. Fillenbaum et al. (1997) combined the results from current meters moored array with the Levitus climatology data and a historical Florida Current data to estimate the meridional heat flux variability at 26.5°N.

Corresponding author address: Dr. Olga T. Sato, Jet Propulsion Laboratory, California Institute of Technology, Mail Stop 300-323, 4800 Oak Grove Drive, Pasadena, CA 91109-8099.
E-mail: sato@pacific.jpl.nasa.gov

Others focus on the transport variability of the Gulf Stream: the site of the largest net oceanic heat losses in the North Atlantic due to the interaction between the warm advected surface waters and the cold and dry continental air masses. The estimates of the amplitude and phase of the annual cycle of the baroclinic volume transport vary. According to Worthington (1976) the volume transport relative to 2000 dbar, calculated from 32 hydrographic sections, has an annual range of 15 Sv (Sv $\equiv 10^6$ m^3 s^{-1}) and is maximum in April. The baroclinic transport at 73°W relative to 2000 m, estimated from the free-falling velocity profiler Pegasus (Halkin and Rossby 1985) has a peak to peak range of about 12 Sv and reaches a maximum in early summer. Sato and Rossby (1995) used 130 historical hydrographic sections and found an annual range of 8 ± 3 Sv with a maximum in summer.

Greatbatch et al. (1991) used the diagnostic model of Mellor et al. (1982) and in situ historical data to investigate the interpentadal changes in the North Atlantic circulation. They found significant changes in the thermohaline structure and circulation between 1955–59 and 1970–74. As a result, the Gulf Stream transport was considerably weaker (by about 30 Sv) during the 1970s compared to the 1950s due to a weakening of the circulation of the subtropical gyre because of changes in the bottom pressure torque associated with the bottom topography. Ezer et al. (1995), using a three-dimensional, free surface, coastal ocean model, corroborate Greatbatch's results. Surprisingly, corresponding interpentadal changes in the poleward heat transport were not detected. They concluded that changes in the sea surface temperature affected the wind pattern, which consequently resulted in changes in the Ekman contribution to the poleward heat transport. Sato and Rossby (1995) studied the low-frequency and seasonal variations in dynamic height anomaly and volume transport of the Gulf Stream using historical hydrographic sections taken during the period from 1932 to 1988. Their upper-layer estimates of the volume transport referenced at 2000 dbar showed a possible 6 Sv decrease from the 1950s to the 1970s.

In this study we investigate the seasonal and decadal variability in the meridional heat flux from historical hydrographic sections that cross the North Atlantic Ocean at 36°N. The North Atlantic basin north of 36°N has two sources of mass: a Pacific inflow at the Bering Strait that makes its way to the Atlantic through the Arctic Ocean and at the southern boundary of the study region at 36°N. The water inflow coming through the Bering Strait is about 1.5 Sv (Coachman et al. 1975) and the corresponding temperature flux through it is negligible (Rago and Rossby 1987). Thus, after accounting for all sources and sinks of water we can establish a closed system in which the net northward mass flux of the upper-layer balances the deep southward returning flow. The volume transport and the temperature flux of the upper layer can be estimated from temper-

ature and salinity (T–S) measurements. By assuming conservation of mass the return deep flow has a volume transport and corresponding seasonal signal that complements the one in the upper layer. Therefore, its temperature flux can be determined by multiplying its volume transport by an average temperature that is representative of the deep layer. Finally, the total meridional heat flux is determined by adding the temperature flux contributions from both layers.

This study is based on direct method in which the amount of heat is estimated by integrating the product of the geostrophic velocity and temperature at each section. By way of reference, the other traditional methods for oceanic heat flux estimation are of a more indirect approach. The surface energy method measures the heat exchange in the air–sea interface using a bulk formula (Bunker 1976; Hastenrath 1980; Lamb 1981; Hsiung 1985), and the global energy method determines the oceanic heat flux as the residual of the radiation balance between the net radiation that reaches the top of the atmosphere and the atmospheric heat flux (Oort and VonderHaar 1976). In both cases the oceanic heat flux is obtained by integrating the estimated heat flux divergence as a function of latitude.

The historical hydrographic data consist of ten transatlantic sections in which two of them sampled the entire basin, vertically and horizontally, while the rest covered the top 2000 m. More transatlantic sections were constructed artificially by connecting sections from four sectors of the ocean near 36°N. The four sectors are the slope water, the Gulf Stream, the Sargasso Sea, and the midocean from the Sargasso Sea to Europe. This method allowed us to expand the data coverage to 60 years and to accurately resolve the seasonal signal for all sectors but the midocean.

The next section outlines the direct method for estimating meridional temperature and heat flux. Section 3 discusses the datasets and their preparation in detail. Sections 4 and 5 discuss the volume and heat fluxes for the various sectors. In section 6 we discuss the strengths and limitations of the estimated results, and the final conclusions are given in section 7.

2. Meridional heat flux

The meridional heat flux due to the ocean currents is estimated by the integral

$$H = \int_0^L \int_0^{z_b} \rho C_p \theta v \, dz \, dx, \tag{1}$$

where ρ is the in situ density of seawater, C_p the specific heat capacity of seawater at constant pressure, θ the potential temperature, L the width of the ocean at the considered latitude, z_b the ocean depth, and v the component of the velocity normal to the section. The product ρC_p is assumed constant (4093 × 10^3 J m^{-3} °C^{-1}). The

large-scale oceanic heat flux is expressed in petawatts, where 1 PW = 10^{15} W.

The meridional heat flux was calculated along the latitude circle of 36°N using historical hydrographic sections. A meaningful estimate of the meridional heat flux requires that Eq. (1) be integrated over a full oceanic section for which there is a zero net mass transport; otherwise the calculated heat transport is dependent on an arbitrary temperature reference (Montgomery 1974). All temperature flux calculations reported here are referenced to 0°C.

A major limitation in using historical datasets is that

$$H = \rho C_p \left\{ \int_0^L \int_0^h (v_{UL} - v_h)\theta_{UL} \, dz \, dx + \int_0^L \int_h^{z_b} (v_{DL} - v_h)\theta_{DL} \, dz \, dx + \int_0^L \int_0^{z_b} v_h\theta \, dz \, dx \right\} + C_p \int_0^L \frac{\tau_x}{f} \theta_{EK} \, dx, \quad (2)$$

where h is an arbitrarily chosen reference depth, in this case 2000 m, thus v_h is the reference current velocity at 2000 m. The index UL refers to the upper layer (above 2000 m), DL refers to the deep layer, and EK refers to the Ekman layer; τ_x is the zonal component of the wind stress and f is the Coriolis frequency.

The first integral (hereafter H_{UL}) is the baroclinic or depth-dependent component of the heat flux. The geostrophic velocity ($v_{UL} - v_h$) is estimated by the dynamic method in which only the relative velocities are known; therefore v_h cannot be determined. To circumvent this problem, the next two integrals, which are the contributions from the deep layer (H_{DL}), are estimated together including a baroclinic as well as a depth-independent velocity component. The last integral (H_{EK}) is the contribution from the direct local response to the wind stress forcing on the Ekman layer.

The integral for the upper ocean is decomposed into four regional sectors, which are the slope water (SW), the Gulf Stream (GS), the Sargasso Sea (SS), and the midocean section from Sargasso Sea to Europe (MO) along 36°N. Equation (2) is then rewritten as

$$H = H_{SW} + H_{GS} + H_{SS} + H_{MO} + H_{EK} + H_{DL}. \quad (3)$$

Each element of the right-hand side of the equation above is referred to as *temperature flux* since the condition of conservation of mass applies only to the expression as a whole. Thus, the expression *heat flux* will be limited to the sum of all temperature fluxes.

3. Data selection and treatment

The area of study is a zonal transect of the North Atlantic Ocean basin approximately at 36°N (Fig. 1). The data come from the *World Ocean Atlas 1994* (WOA94) (Levitus and Boyer 1994), distributed by the National Oceanographic Data Center (NODC), and con-

the temperature and salinity profiles typically do not extend to the bottom. Uniform vertical sampling was achieved by limiting all profiles to 2000-m depth. This depth was chosen because (i) most hydrocasts went this deep, (ii) variability is expected to be small below this level, and (iii) because (for the same reasons) it has been chosen previously as a reference level (Worthington 1976; Sato and Rossby 1995), thus facilitating comparison of results.

To analyze the different contributions associated with distinct components of the total heat flux, the integral in Eq. (1) was rewritten as

tain global ocean temperature and salinity profiles taken between 1900 and 1990. Hydrographic sections from bottle casts were preferred for the investigation of a long-term variability because they have been taken since the 1930s (Table 1). An additional dataset (RU) from repeated sections across the Gulf Stream between 1972 and 1981 was provided by the State Oceanography Institute in Moscow, Russia. Some of these Russian sections can be found in the WOA94 dataset.

All temperature and salinity profiles were linearly interpolated to the 29 NODC standard depths levels. For the interpolation, pressure was converted to depth using either a constant value of gravity for the WOA94 data or gravity as a function of latitude for the RU data. The vertical interpolation scheme for missing points in the temperature profiles is similar in all sectors. Missing surface data (above 100 m) were extrapolated by repeating the first measured value upward under the assumption that the missing data were within the mixed layer. Missing values between the mixed layer and the thermocline were estimated by using the vertical gradient of the closest profile in the section. Missing values in the middle of the profile were estimated by linear interpolation (stations with a gap larger than 200 m in the thermocline layer were discarded).

For the slope water and the Sargasso Sea sectors, missing values in the deeper part of the profiles (below 1400 m) were estimated by extrapolation using the mean temperature gradient. All complete temperature profiles in the section were averaged together to obtain a mean profile from which the vertical gradients were determined. For the Gulf Stream sector, to extrapolate the profile below 1400 m two distinct mean temperature gradients were used, one for each side of the stream. The point chosen to divide the stream was halfway between where the 12°C isotherm reached the depths of 400 and 600 m. For the midocean and transatlantic sec-
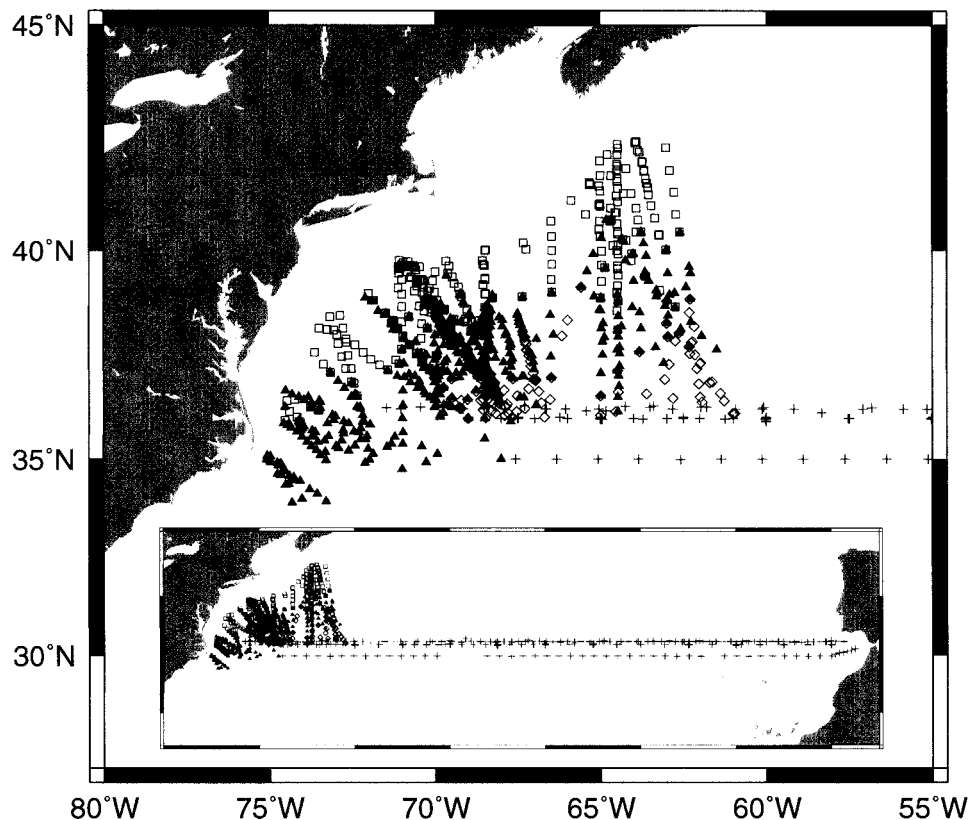
FIG. 1. Location of the stations in the slope water (squares), Gulf Stream (triangles), Sargasso Sea (diamonds), and midocean (plus signs) sectors.

tions, temperature and salinity profiles shallower than 1400 m were extended to 2000 m by using temperature and salinity gradients bin averaged over 5° of longitude.

Gaps in the salinity profiles for the sectors in the western side of the Atlantic were filled using linear interpolation and the Armi–Bray algorithm was used for extrapolation (Armi and Bray 1982). This algorithm reproduces a mean potential temperature and salinity relationship curve for the western North Atlantic. Salinity corresponding to the applicable temperature range (0.5° to 20°C) was interpolated or extrapolated using the empirical salinity gradient estimated by the algorithm. Outside that range of temperatures (usually near the surface), the data were interpolated linearly if there was a salinity gap or just repeated upward in case of an extrapolation, assuming again that the missing data were within the mixed layer.

TABLE 1. Distribution of the data in time and the number of sections (N) used in each sector.

Sector	Period	N
Slope water	1931–86	103
Gulf Stream	1922–86	140
Sargasso Sea	1931–80	138 (74)
Midocean	1970–81	10
Transatlantic	1959, 1970–81	11

The precision of the interpolation/extrapolation method was tested by superimposing the observed T–S diagram on the empirical Armi–Bray T–S curve. The interpolated points lying outside an envelope of more than two standard deviations around the empirical curves were replaced by their empirical values if it did not cause a discontinuity or inversion in the salinity profile, otherwise the whole station was discarded.

a. Slope water and Sargasso Sea

In the western side of basin the selected stations belong to sections that span the whole region from the slope water, across the Gulf Stream up to the Sargasso Sea (line AC in Fig. 2). Then, the last (southmost) station in the Sargasso Sea was directly connected to the closest intercepting point in the mean midocean section. This procedure assures that, once all the partial sections are connected, they draw a continuous line along the Atlantic, thus closing the basin. Given this consideration, a total of 103 sections were available connecting the slope water and the Gulf Stream sectors with an average of five stations per section. Initially, 74 sections south of the Gulf Stream that cover as much of the Sargasso Sea as possible were selected, with an average of four stations per section.
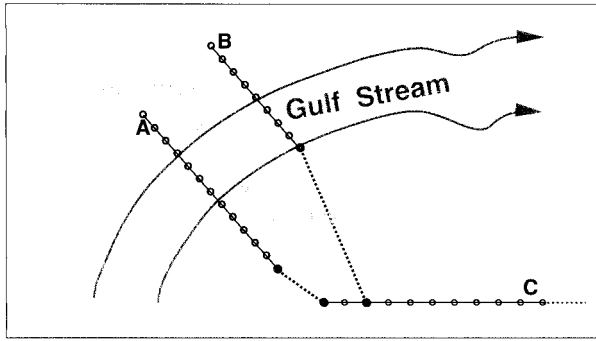
Fig. 2. Illustration on connecting the sections in the western Atlantic (A and B) to the closest station in the mean midocean section (C).
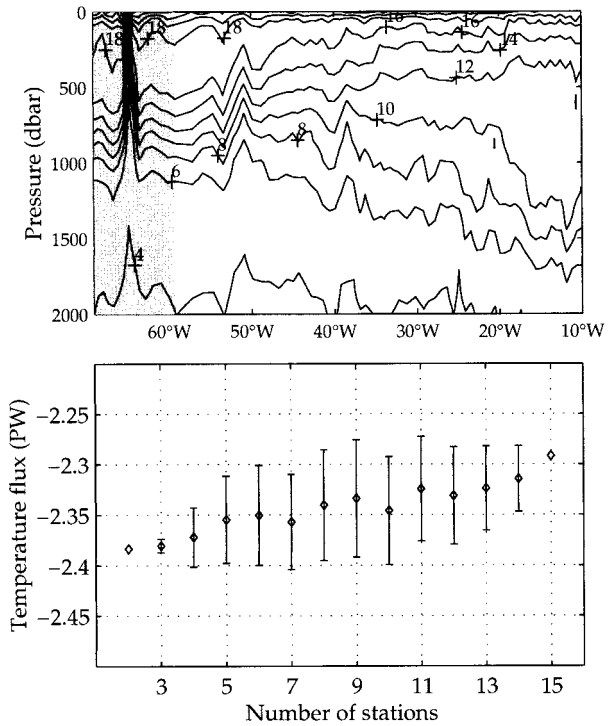

Fig. 3. Temperature contours in the 1981 transatlantic section (top panel). The highlighted region represents stations 17–31 where the sensitivity test of the temperature flux to the horizontal resolution (bottom panel) was performed. The error bars correspond to the standard error from up to 300 independent realizations.

Based on the fact that the volume transport depends on the two outermost stations in the section and that the seasonal cycle in the Sargasso Sea is small, more sections for this sector could be included. Besides the 74 sections already selected, there were 64 more that have one station in common between the Gulf Stream and the Sargasso Sea sectors. This single station can be directly connected to the closest station in the midocean sector (line BC in Fig. 2).

The width of these single-station Sargasso Sea sections varies: the mean width is about 150 km, however, in 19 cases the gap is larger than 300 km and the largest separation is about 600 km. The error introduced by using sections with poor horizontal resolution could result in a slightly inaccurate estimate. A Monte Carlo simulation is done to test the sensitivity of the temperature flux estimates to the horizontal resolution in the Sargasso Sea. The 1981 section (Roemmich and Wunsch 1985), specifically its western side, was chosen because of the high horizontal resolution (top panel in Fig. 3). There are 15 stations in the highlighted region originally labeled with station numbers from 17 to 31. The segment is 900 km long with 64 km between stations on average. The temperature flux through stations 17 to 31 is -0.23 PW. In the simulation the temperature flux is recalculated for a decreasing number of stations, n, varying from 15 down to 2 stations (the ones at the edges are always included). The temperature flux is estimated for up to 300 different random combinations of n stations.

The difference between considering all stations or only two is 0.09 PW, (bottom panel in Fig. 3), or 11% of the 0.8 PW total oceanic heat flux determined by Roemmich (1980). This value was obtained for a region 900 km wide, approximately six times larger than the actual Sargasso Sea sector. Therefore, including less resolved sections in the Sargasso Sea should not have a significant impact in the total heat estimates, as 11% can be taken as an upper limit of the error estimates.

b. Gulf Stream

The isotherms on a typical cross-stream profile are shallow on the slope water side and deep on the Sargasso Sea side. The position of the northern edge of the stream is defined as the station just north of where the slope of the isotherms increases sharply downward, which coincides with the cross-stream position where the 12°C isotherm is about 150 m. The southern edge of the stream is defined as the location where the isopycnals become level, corresponding roughly to the point where the 12°C isotherm is nearly 800 m deep. All sections have been selected so they are not contaminated by the presence of rings that show up as large amplitude changes in depth of the isotherms or isopycnals. After the quality check and interpolation, a total of 789 stations in 140 sections were retained.

The number of stations in each section varies. Some sections have more than 10 stations within the stream separated by less than 20 km. Most sections have between 4 and 8 stations with an average separation of 50 km. A few sections (18) have only 3 stations intersecting the stream: two stations bracketing the current and one station between them. Although these sections are undersampled, their location, T–S properties, and temperature stratification suggest that they represent a Gulf Stream cross section, and therefore they were used. That the horizontal resolution is nonuniform does not affect

the geostrophic transport estimates because the transport across a section is proportional to the potential energy anomaly difference between the two outermost stations (Sato and Rossby 1995).

In contrast to volume transport, the horizontal resolution does affect the estimation of the heat flux since it results from the direct integration of the product of temperature and velocity fields. An integration by a finite differences method between two stations implicitly employs a linear interpolation. Whenever the section in question is poorly sampled, a linear interpolation can systematically introduce errors in the temperature flux estimates.

The temperature structure of the Gulf Stream has a strikingly regular shape. The distribution of the isotherms in the cross-stream direction presents a consistent pattern throughout the year. This quasi-rigid shape has been used by various authors (Hogg 1986; Hendry 1988; Bower and Rossby 1989; Hogg 1991; Hall 1994) to analytically reproduce the temperature and velocity fields. The function often used to describe the cross-stream distribution of the isotherms of the Gulf Stream is the hyperbolic tangent.

This basic or "canonical" shape of the Gulf Stream is less evident when the section is undersampled. In practice, a section is sampled horizontally at only a few discrete points (top panel in Fig. 4). In this case, the isotherm obtained by connecting a few points across the stream (line A in Fig. 4) is shifted from the idealized curve (line B). An artifact from the linear interpolation is that the depth of the isotherms as a function of the cross-stream coordinates tends to be shallower than prescribed on the Sargasso Sea side and deeper on the slope water side of the stream. The error in the determination of the isotherm depth increases with decreasing number of stations. Consequently, the linear interpolation consistently decreases the temperature gradient across the stream, underestimating the normal component of heat flux. A sensitivity test is done based on a well-sampled section of the Gulf Stream to evaluate the effect of the horizontal resolution on the estimation of the heat flux (or temperature flux).

The CTD section described as line I by Johns et al. (1989), chosen for its high-resolution sampling, is used to estimate the sensitivity of the temperature flux estimates to the horizontal resolution. The CTD line I was taken near 73°W perpendicular to the mean path of the Gulf Stream on July 1982. This section has 11 stations separated by approximately 25 km (in the central high velocity core the separation is 10–12 km). The depth of the cast is limited to 2000 m with a vertical resolution of 10 m. To be consistent with the historical hydrographic sections the section was vertically interpolated to the standard depths. The baroclinic transport referenced at 2000 m is 73 Sv and the corresponding temperature flux is 4.84 PW. Keeping the two stations at the edges, the temperature flux is estimated by varying the number of stations from 1 to 9. The stations were
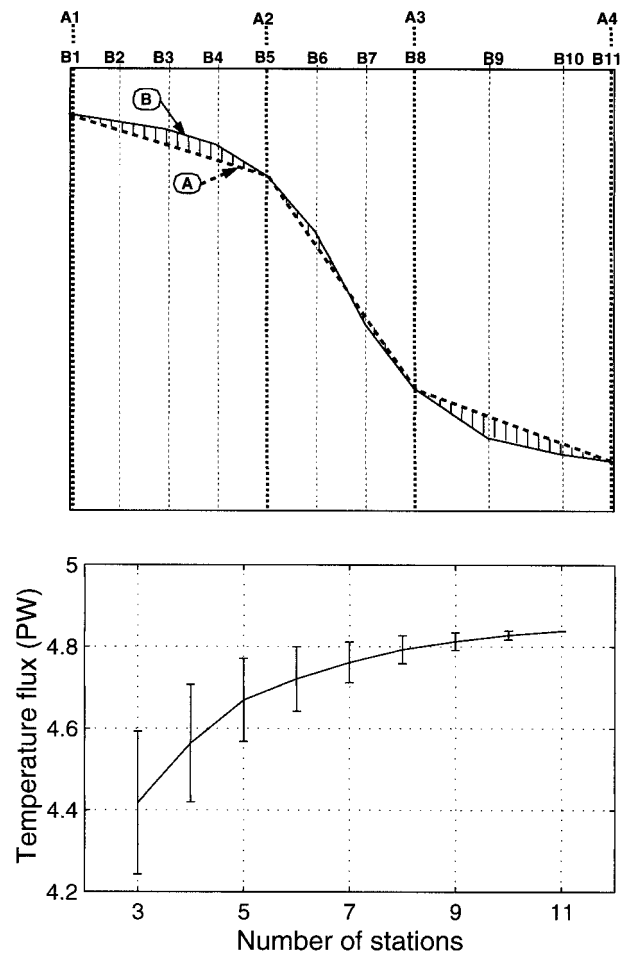

FIG. 4. The stippled area (top panel) represents the difference in the thermocline depth in a highly sampled (line B) and a less resolved section (line A). Monte Carlo simulation (bottom panel) for the sensitivity test on the temperature flux to the horizontal resolution for a CTD section. The error bars represent the standard deviation for up to 300 realizations for each specific number of stations (N).

picked randomly and a Monte Carlo simulation using up to 300 combinations was performed for a given number of stations. The difference in the mean temperature flux between 3 and 11 stations was 0.4 PW (bottom panel in Fig. 4).

The temperature flux tends to decrease as the horizontal resolution decreases. Conversely, the standard deviation decreases and the mean value tends to the control value as the resolution increases. Hence, to avoid a downward bias of temperature flux estimates when only sparse data are available, we use a parametric interpolation method based on a hyperbolic tangent function to reconstruct the full temperature structure of the Gulf Stream (Sato 1997).

c. The midocean

Twenty sections, ten of transatlantic extension and ten just across the midocean sector, were used. These

sections usually go from 10° to 69°W longitude. The vertical sampling was not uniform: some sections were surveyed by alternating deep stations (deeper than 1400 m) with shallow stations (only up to 800 m). In these cases, only the deeper stations were used for the calculations, interpolated or extrapolated as needed; the shallow stations were excluded.

The mean baroclinic transport is estimated by using the mean potential energy anomaly between 10° and 69°W. The transport of the mean section is −33 ± 13 Sv. The seasonal cycle of the transport across the midocean sector cannot be determined with accuracy. The determination of the transport is subject to large variability as there are only few sections in the sector.

To evaluate the relative importance of the eddy field, the baroclinic component of the temperature flux ($v\theta$) was divided into two contributions: the temporal mean ($\overline{v\theta}$) and the correlated eddy field ($v'\theta'$). These products are integrated from the eastern limit of the grid at 10°W to the western limit at 69°W. To avoid bias due to the intense eddy field near the western boundary current and sections that end in the middle of an eddy, the temperature flux was integrated to the longitude where the integral of v' (fluctuations in the transport due to the eddy field) is as close to zero as possible. The temperature flux due to the mean velocity and temperature fields is 2.0 PW to the south. The mean contribution of the eddy field to the temperature flux is 0.06 PW to the north. Although small, it will be included in the mean midocean sector. As a result, the temperature flux of the midocean sector is −1.9 PW.

d. The transatlantic sections

A total of ten transatlantic sections were selected from the WOA94 dataset. Among them there was the 1959 section taken during the International Geophysical Year (IGY) and the 1981 section described by Roemmich and Wunsch (1985). Of the ten sections, eight were surveyed by the former Soviet Union (FSU) ships. Uncertainties in the salinity measurements are the major source of error on the FSU cruises. Among these cruises, only sections with T–S characteristics in agreement with the water masses in the North Atlantic region were used.

Most of them are composed of two segments, one oriented zonally going from 10° to 70°W and the other one angled toward the northwest reaching the 2000-m isobath, always crossing the Gulf Stream path. In contrast, the 1959 IGY goes straight from Europe to the American continent. In two 1980 sections after the ships surveyed the midocean portion, they headed southeastward to Bermuda and then turned to the northwest again, until crossing the Gulf Stream. For these two cases, the stations in the segment between Bermuda and 36°N were excluded.

The average horizontal separation between stations varies. The best horizontal resolution is from the 1981 section with 70 km of separation, followed by the IGY

section with 140 km, then the sections from 1977 to 1980 with 220 km, and finally for the 1972–76 sections the mean separation is 500 km. The sections span the entire width of the basin except for a region between the 2000-m isobath and the shelf break on both sides of the ocean. The transport across the extreme east side of the basin is estimated by extrapolating the velocities east of 10°W from eight sections from the transatlantic and midocean sector. The volume flux was estimated to be less than 1 Sv (to the north) on the eastern side and 1 Sv (to the south) on western side (Luyten 1977).

4. Volume transport

The baroclinic volume transport for the upper layer across the sectors was estimated by the potential energy anomaly method, discussed in Sato and Rossby (1995).

The estimate of the annual signal is affected by factors such as the eddy field, spatial distribution of the stations relative to the downstream position, and distribution of samples in time. The sampling of the sections is not uniform in time. Therefore, the annual mean can potentially contain a temporal bias that can be prevented by estimating the total mean from seasonal averages. The temporal bias in the volume transport of the SW, GS, and SS are individually determined and removed. For instance, in the Gulf Stream there are 84 sections taken during the spring/summer months and 56 sections during the fall/winter period. In this case, the annual mean of the volume transport is calculated by averaging the mean of the spring/summer and the mean of the fall/winter months.

In the western side of the basin the selected sections are normal to the current and extend about 500 km in the downstream direction north from 36°N. Therefore, some adjustments in the volume transport are required so that the final result would represent the fluxes through the 36°N latitude line and not through the oceanic transect. The spatial bias in the volume transport in the SW, GS, and SS sectors combined relative to 36°N is −2.6 Sv/100 km. This bias is estimated by linear regression, and the transport across the section is projected to 36°N. All the results shown hereafter reflect this bias correction. As a reference, the annual mean of the UL volume transport increased by 3.7 Sv from its initial (biased) estimates.

The seasonal signal for the transport of the Gulf Stream has a maximum in early summer and an amplitude of 11 ± 5 Sv (Fig. 5 and Table 2). In all cases, the annual cycle, the mean for every two-month bin and the corresponding standard error of the mean, when the number of sections in the bin is larger than 10, are superimposed onto the data.

In the slope water sector the seasonal signal is hardly distinguishable from the eddy fluctuations. Although small, the volume transport exhibits a southward volume flux in the summer. It appears that most of the seasonal variation in baroclinic transport in this sector is domi-
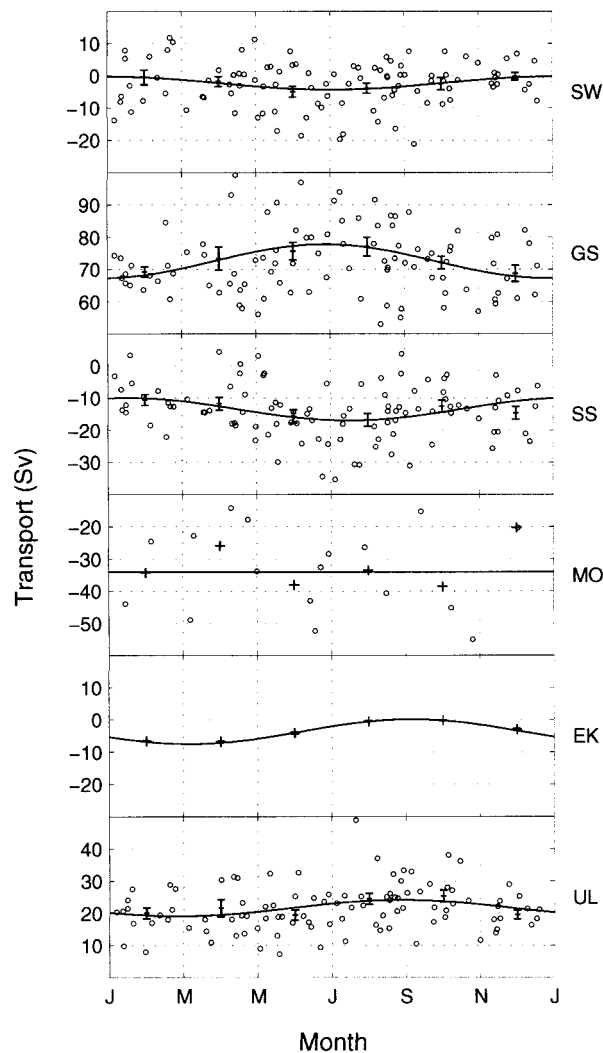
FIG. 5. Annual cycle of the volume transport in the upper layer at 36°N. The volume transport of the upper layer is $V_{UL} = V_{SW} + V_{GS} + V_{SS} + V_{MO} + V_{EK}$ [plus transport from the Bering Strait and the continental rises (not shown)]. The data are shown in circles, plus signs are the 2-month bin averages, and the error bars representing the standard error of the mean are superimposed when at least 10 sections are available. The continuous line is the sinusoidal fit for the annual cycle except for the MO where the transport is constant (-33 Sv).

TABLE 2. Annual cycle mean and range of the transport (Sv) in the upper layer at 36°N. A negative mean annual transport implies a southward flow.

Region	Mean	Range
SW	-3 ± 7	4 ± 3
GS	73 ± 11	11 ± 5
SS	-14 ± 8	7 ± 3
MO	-33 ± 13	—
EK	-3	8 ± 1
Western rise	-1	—
Eastern rise	1	—
Bering Strait	1.5	—
UL	22 ± 8	5 ± 3

The volume transport in the Ekman layer was obtained for the entire transoceanic section at the latitude line 36°N using monthly maps in a $1° \times 1°$ grid from the Bunker climatological atlas (Isemer and Hasse 1987). The meridional component of the Ekman transport through each 1° box for each month was zonally integrated across the basin. At 36°N, the annual mean Ekman transport was estimated to be 3 Sv to the south, a range of 8 Sv, and a southward maximum was found in the late winter.

Since the number of sections in the SW, GS, and SS sectors are not the same, the upper-layer volume transport (V_{UL}) is estimated by adding the contribution from 100 sections that are common for the three sectors. Here V_{UL} also includes a constant midocean transport, the Ekman transport, and the small contributions from the Bering Strait and the continental rises from both edges of the basin as listed on Table 2. The result is a net northward flow of 22 ± 8 Sv and an annual range of 5 ± 3 Sv with a maximum in the late summer (Fig. 5).

To analyze the low-frequency changes, the transport residuals averaged in pentads (period of five years) were plotted as a function of year for all sectors (Fig. 6), excluding the outliers of 1.5 standard deviation relative to its seasonal cycle fit. Due to the large scatter, especially after the 1970s, the errors represent the standard error of the mean within the pentad (the error bar is shown only for the pentads with at least 10 sections). The increased number of sections observed after the 1970s is due to the contribution from the RU sections.

The long-term variability is more evident in the transport of the Gulf Stream alone than in the sum of other contributions. The low-frequency variations in the transport of the Gulf Stream of Sato and Rossby (1995) can be verified in this study, which uses a more strict criterion, that is, the pentads have to have at least ten sections to be considered. They observed a decrease of 6 Sv in the transport residual between the 1955–59 and 1970–74 pentads. In this study, because of the insufficient number of sections in the 1955–59 pentad, its mean transport residual cannot be determined with confidence. The transport residual in the Gulf Stream increases by 10 Sv between the early 1960s and the early

nated by the seasonal changes in the main thermocline. The seasonal cycle in transport of the Sargasso Sea is about one month out of phase with that of the Gulf Stream, but this phase lag is not well established. The maximum southward transport in the Sargasso Sea is also in summer.

An important result from the volume transport analysis is that the seasonal cycle in the added transport of the slope water and Sargasso Sea almost cancels out the seasonal cycle of the Gulf Stream (Table 2). Indeed, the total transport across the three sectors has an annual mean of 57 ± 8 Sv and a statistically insignificant annual cycle of 3 ± 3 Sv.
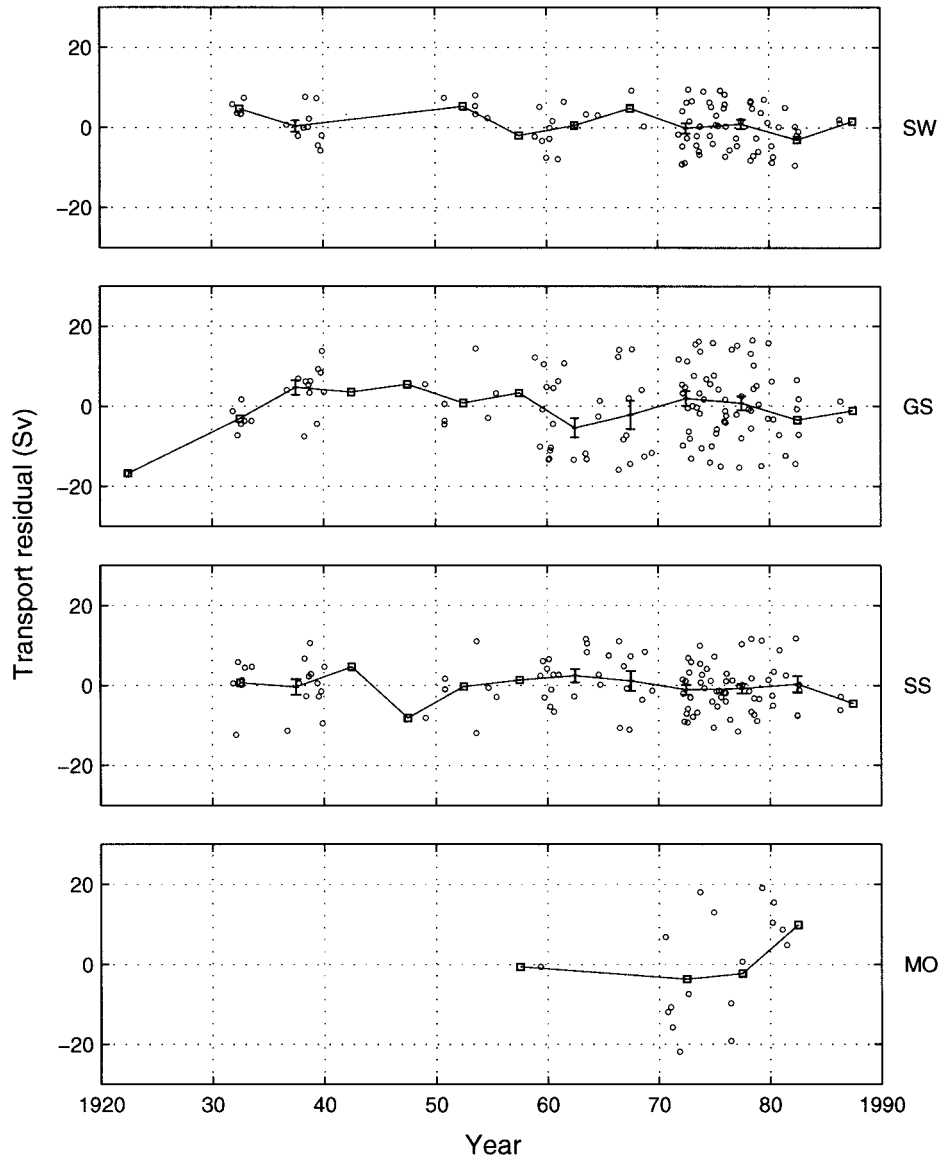
FIG. 6. Low-frequency variability in the upper-layer baroclinic volume transport residuals (transport estimates minus the seasonal cycle fit, except for the MO where only its mean is removed). The error bars are shown for pentads with more than 10 sections and represent the standard error of the mean. The squares represent the mean for pentads with less than 10 observations.

1970s, followed by a decrease of 6 Sv toward the mid-1980s. In the Sargasso Sea sector, although in smaller amplitude, the low-frequency changes are exactly the opposite. Only one pentad before the 1960s was considered statistically significant: the period between 1935 and 1940.

For the slope water and the midocean sectors the number of observations is insufficient to draw any conclusions about the low-frequency changes between pentads in the transport residual, except for the 1970s in the slope water where no significant changes are observed.

5. Heat flux

Analogously to the volume transport, the temperature flux in the upper layer is estimated by adding the contributions from the four sectors to the temperature flux of the Ekman layer, (Fig. 7). The temperature flux of the Bering Strait inflow and across the continental rises are considered negligible.

As mentioned in section 4, the spatial bias in the volume transport due to the location of the sections relative to 36°N is small. However, the spatial bias of the heat flux could be relatively large, not only because
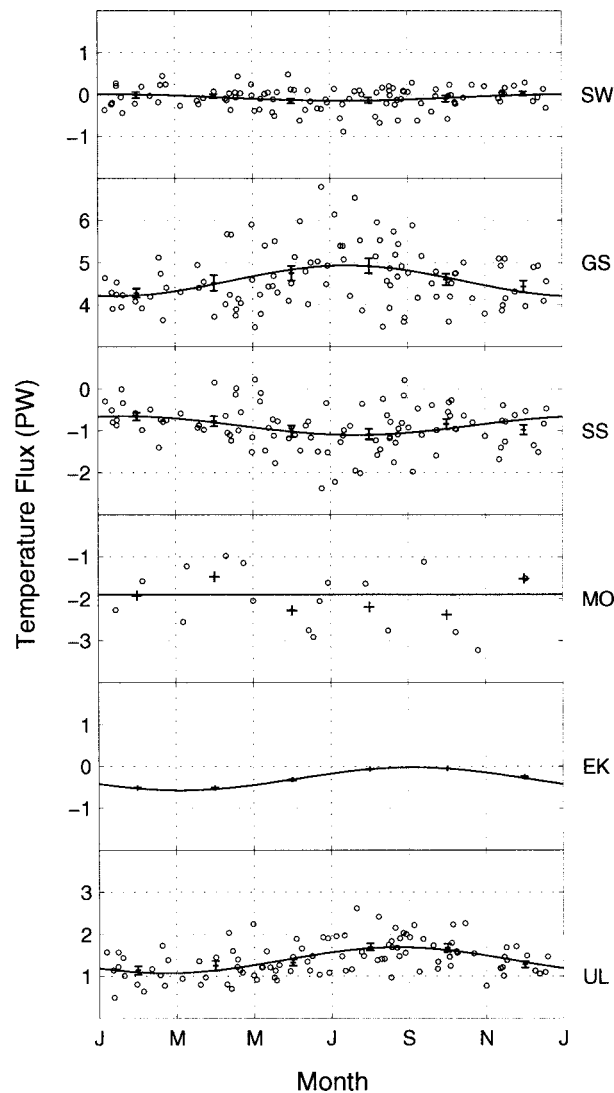
FIG. 7. Same as Fig. 5 but for temperature flux in the upper layer. Temperature flux for MO is constant in time (−1.9 PW).

deep flow is mostly carried by the deep western boundary current (DWBC), while the midocean deep waters move at a relatively slow (and poorly known) pace rather than a uniform southward flow.

The condition of mass conservation means that any fluctuation in the upper-layer transport would be directly counterbalanced in the deep layer. This method allows us only to estimate the integrated volume transport for the deep layer (V_{DL}) and its temporal variability but not its velocity field. Therefore, the temperature flux is just the product $V_{DL}\overline{\theta}$, where V_{DL} is $-V_{UL}$ and $\overline{\theta}$ is the mean potential temperature of the DWBC. The dynamics and structure of the DWBC were studied by Pickart and Watts (1990) using an array of inverted echo sounders and bottom current meters off Cape Hatteras, where the Gulf Stream and the DWBC cross each other. In this region the DWBC core was found at a depth of 3000–3500 m, with a potential temperature of 2.0°–2.5°C. The temperature used here to estimate the temperature flux for the deep layer was the average, 2.3°C.

The total oceanic heat flux at 36°N, estimated by adding the temperature flux of the upper and deep layers, has a northward resultant net flow with a mean magnitude of 1.2 PW (Fig. 8) and a standard deviation of 0.3 PW, as discussed in appendix B. The peak to peak range of the seasonal cycle is 0.6 ± 0.1 PW with a maximum in the late summer (Table 3). Initially, the annual cycle model used all available points (from the 100 sections) to obtain a sinusoidal fit. Six outliers (outside a two standard deviations envelope) were excluded from the data. The remaining points were submitted again to the least squares fit procedure to estimate the amplitude of the annual cycle. For consistency check, the temperature flux estimates from the ten transatlantic sections are superimposed on data in Fig. 8.

The main contribution for the net northward heat flux comes from the baroclinic temperature flux of the Gulf Stream. However, the seasonal cycle is in phase with the Ekman temperature flux. The baroclinic temperature flux of the Gulf Stream is almost 180° out of phase with the temperature flux of the slope water and the Sargasso Sea. Those three sectors combined contribute with a seasonal cycle range of 0.1 PW. Since the seasonal signal from the midocean is not well established and therefore ignored, the annual range of 0.5 PW from the Ekman layer dominates.

To verify the significance of the seasonal signal in the heat flux the Wilcoxon rank sum test for two independent samples was applied (Wall 1986). The technique compares two distinct data distributions and tests the validity of the null hypothesis, that is, that the two sample distributions differ only by chance. Here, the two distinct sample distributions are the two halves of the year, each corresponding to a six-month period centered around the points of maximum and minimum obtained by the fit. The median of the heat flux for the first period, from June through November, is 1.3 PW and has 51 points, while the other half has a median of

the Gulf Stream is responsible for large oceanic heat losses to the atmosphere but also because these losses vary meridionally. The spatial bias in the temperature flux of the SW, GS, and SS sectors combined is estimated by linear regression and the temperature flux of each individual section is projected to 36°N. The estimated bias is −0.2 PW/100 km. All the results shown hereafter reflect this correction and thus represent the values adjusted to 36°N. For reference, the annual mean of the heat flux increased 0.2 PW in relation to its initial (biased) estimates.

The northward flow of the upper layer should, by conservation of mass, be compensated by a southward flow at depth. Thus, the seasonal cycle of the deep return flow should complement the one observed in the upper layer. To be consistent with present ideas about the thermohaline circulation, it is reasonable to assume that the
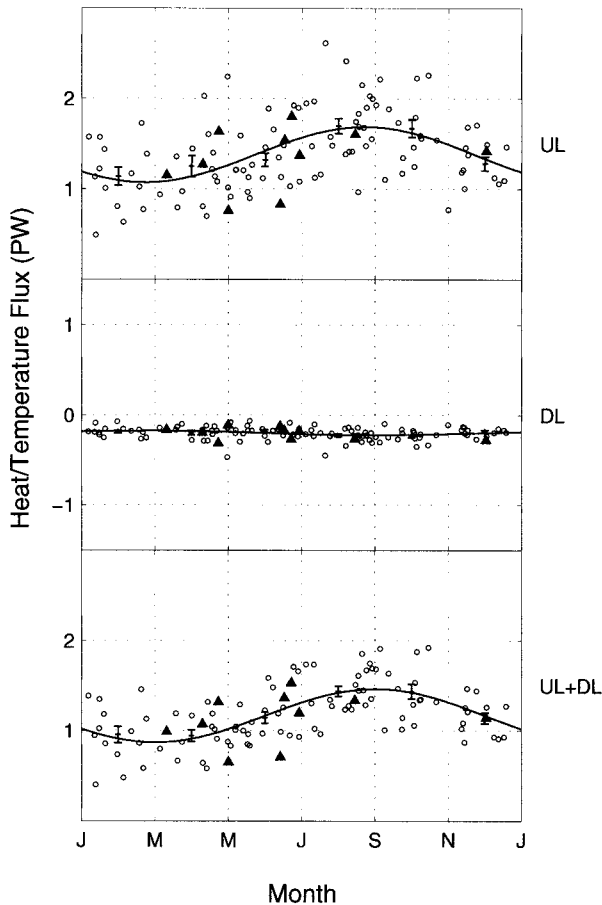
FIG. 8. Annual cycle in the temperature flux of the upper layer (UL), the deep layer (DL), and the total oceanic heat flux (UL + DL). The data are shown in circles and error bars are centered at 2-month bin averages representing the standard error of the mean when at least 10 sections are available. Estimates from the ten transatlantic sections (triangles) are included.

1.0 PW with 43 points. Therefore, according to the Wilcoxon test, the two distributions are statistically different from each other above the 95% level of confidence.

6. Discussion

In the introduction three methods of estimating poleward heat transport were mentioned. For example, the surface heat flux method can estimate the latitudinal distribution of heat flux, but the method depends sensitively upon the accuracy of bulk formula in estimating the various contributions to the surface heat flux. The advantage of the surface fluxes method is that it immediately gives a picture of the latitudinal distribution of heat flux (Bunker 1976; Lamb 1981; Hsiung 1985). The direct method of estimation, as used here, yields only single estimates, one for each section, but is almost certainly more accurate (Table 4). Therefore, it is essential to obtain sections from throughout the year in

TABLE 3. Annual mean and range of the temperature flux and the total heat flux at 36°N. Positive values denote northward flux expressed in PW.

Sector	Mean	Range
SW	-0.1 ± 0.2	0.2 ± 0.1
GS	4.6 ± 0.6	0.7 ± 0.3
SS	-0.9 ± 0.5	0.5 ± 0.2
MO	-1.9	—
EK	-0.3	0.5 ± 0.1
UL	1.4 ± 0.3	0.6 ± 0.1
DL	-0.20 ± 0.06	0.05 ± 0.02
Total	1.2 ± 0.3	0.6 ± 0.1

order to identify the annual component's contribution to the poleward heat flux.

To put the results of this study into perspective, the heat flux is plotted in Fig. 9 along with those from a number of studies, including the estimates based on climatological air–sea surface fluxes by Bunker (1976), Lamb (1981), which includes an error estimate, and by Hsiung (1985), and various single points estimates in the Atlantic (Bennett 1978; Bryan 1962; Fillenbaum et al. 1997; Molinari et al. 1990; Hall and Bryden 1982; Rago and Rossby 1987; Roemmich and Wunsch 1985).

Rago and Rossby (1987, hereafter RR) used a methodology similar to this study by dividing the basin into six sectors at 32°N. The result was a northward heat flux of 1.38 ± 0.19 PW (Table 4), a peak to peak annual range of about 0.8 PW with a maximum in the summer. The difference between 1.38 PW at 32°N and 1.2 PW at 36°N by the present study results from physical processes. The difference can be explained in terms of the meridional change in the typical oceanic heat losses and Ekman components. These results corroborate the surface energy fluxes from climatological data in Fig. 9, which shows a decrease of about 0.14 PW between 32° and 36°N.

Next, we examine the sources for the difference in the amplitude of the annual cycle of the heat flux between both studies. Rago and Rossby found an annual range for the temperature flux in the Gulf Stream of about 1.0 PW, using 19 Pegasus sections taken within

TABLE 4. Northward oceanic heat flux (in PW) for the Atlantic Ocean. (Multiple values refer to measurements from different data sources.)

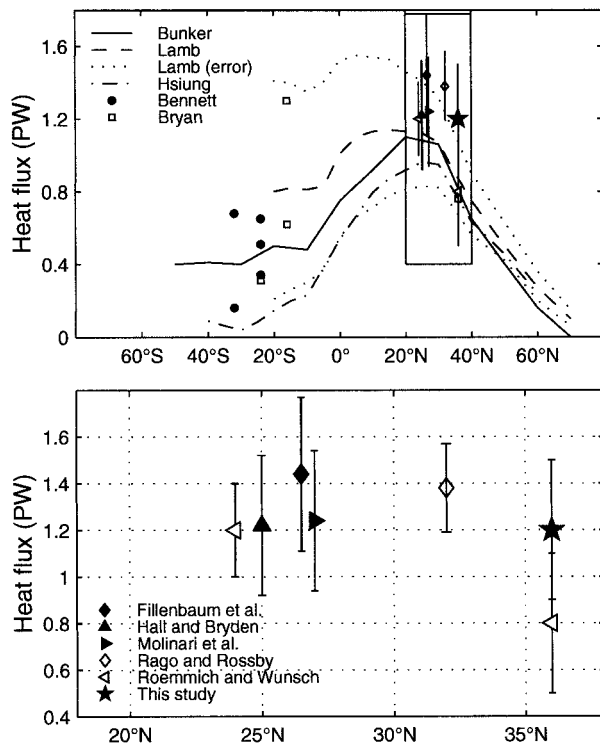| Study	Heat flux	Location
Bennett (1978)	0.34, 0.51, 0.65	24°S
	0.16, 0.68	32°S
Bryan (1962)	0.31	24°S
	0.62, 1.3	16°S
Fillenbaum et al. (1997)	1.44 ± 0.33	26.5°N
Molinari et al. (1990)	1.21 ± 0.34	26.5°N
Hall and Bryden (1982)	1.22 ± 0.3	24.5°N
Rago and Rossby (1987)	1.38 ± 0.19	32°N
Roemmich and Wunsch (1985)	1.22	24.5°N
	0.8	36°N
This study	1.2 ± 0.3	36°N

FIG. 9. Northward oceanic heat flux for the Atlantic Ocean. Bottom panel is an expanded view of the selected region in top panel.

a 2½ yr period. The combined seasonal variations of the temperature flux in the Gulf Stream and in the Ekman layer were used to infer a seasonal cycle for the midocean sector, which in their study was represented by a single section. The annual cycle in the temperature flux from the slope water and Sargasso Sea sectors are small and, therefore, according to RR, as a result the seasonal signal from the Gulf Stream dominates the heat flux for the North Atlantic.

For this study, the seasonal cycle of the temperature flux for the slope water and the Sargasso Sea have significant amplitudes. The annual cycle of the temperature flux of the Gulf Stream is almost canceled out by the seasonal signal of the temperature flux from the slope water and Sargasso Sea. The estimated seasonal cycle of the Ekman temperature flux becomes the dominant contributor to the annual variation in poleward heat flux. Although RR's heat flux seasonal range is larger than ours, the phase is similar.

Figure 10 shows low-frequency changes in the temperature flux residual for the upper layer (top panel), deep layer (middle), and in the total heat flux residual (bottom). To evaluate if the variability observed in the residual is significant we have to know the error associated with the heat estimates (discussed in appendix B). The error in the heat flux estimates is 0.3 PW. This means that only low-frequency changes larger than that are significant. For the three pentads for which there are

at least ten sections (1935–39, 1970–74, and 1975–79), the means agree to within 0.1 PW.

The use of an interpolation scheme to improve the horizontal resolution of the Gulf Stream sections had a considerable impact in the determination of the total heat flux. The sensitivity test performed for a Gulf Stream section (Fig. 4) showed that the temperature flux tends asymptotically to a more accurate value as a function of the horizontal resolution. This tendency is extrapolated to all Gulf Stream sections where the temperature fields are horizontally interpolated using a parametric model based on a hyperbolic tangent function. As a result, the interpolated sections reproduce a more realistic curvature of the temperature field and on average increased the temperature flux estimates by 0.3 PW (Fig. 11).

7. Conclusions

Historical hydrographic sections, spanning about 60 years of data, have been used to investigate the seasonal and low-frequency variability in volume transport and heat flux of the North Atlantic Ocean at 36°N. The available hydrographic sections enclose distinct oceanic sectors that, when connected, close the entire basin. Those sectors are the slope water, the Gulf Stream, the Sargasso Sea, and the midocean sector from the Sargasso Sea to Europe. Conceptually, a section is required to have a zero net mass transport; otherwise the calculated heat flux is dependent on an arbitrary temperature reference. This condition is satisfied for the North Atlantic Ocean, which is approximately closed to the north except for a small flow through the Bering Strait. Following are the summary of the results and the conclusions.

1) A parametric interpolation method based on the hyperbolic tangent to represent the temperature field was used to interpolate the Gulf Stream sections to increase the horizontal resolution. The relationship between its temperature and velocity structure makes the estimation of temperature flux sensitive to the horizontal resolution. On average, the temperature flux of the Gulf Stream was increased by 0.3 PW.

2) The seasonal cycle in the volume transport of the Gulf Stream has an amplitude of 11 ± 5 Sv with a maximum in the early summer. The seasonal signal is significant for the slope water and Sargasso Sea sectors, their combined seasonal signal almost cancels out that of the Gulf Stream. This result corroborates what is already known about the gyre dynamics. The seasonal signal in the midocean was not determined because of the uncertainty resulting from the scarce number of observations in this sector.

3) The total baroclinic transport of the layer above 2000 dbar has a net northward flow of 23 ± 8 Sv (the error is the standard deviation and does not include the seasonal variability). The range of the annual cycle is 3 ± 3 Sv. At 36°N, the annual mean Ekman
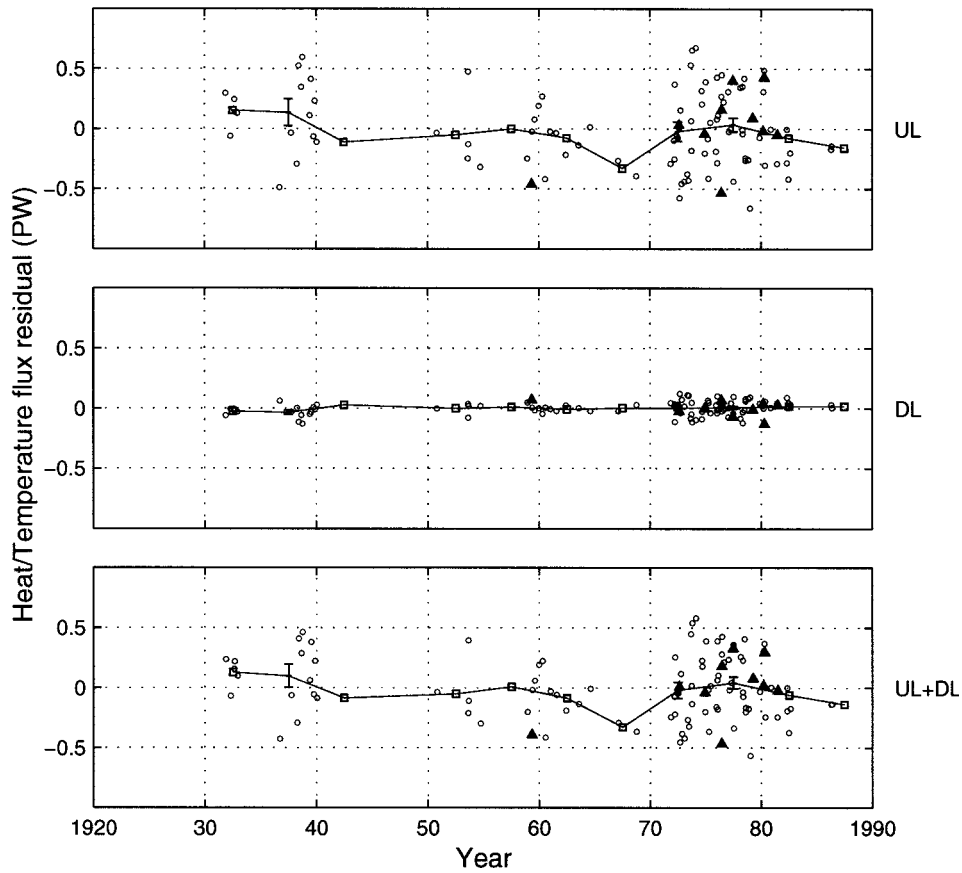
FIG. 10. Low-frequency variability in the temperature flux of the upper and deep layer and the total heat flux residuals relative to 2000 dbar (data shown in circles). The error bars (standard error of the mean) are shown for pentads with at least ten sections and squares otherwise. Triangles represent the residuals estimated from the ten transatlantic sections.

transport is 3 Sv to the south with a range of 8 Sv with a maximum southward transport in late winter. The total upper-layer transport, which includes the baroclinic transport plus the Ekman, Bering Strait transports, and the flow from the continental rises
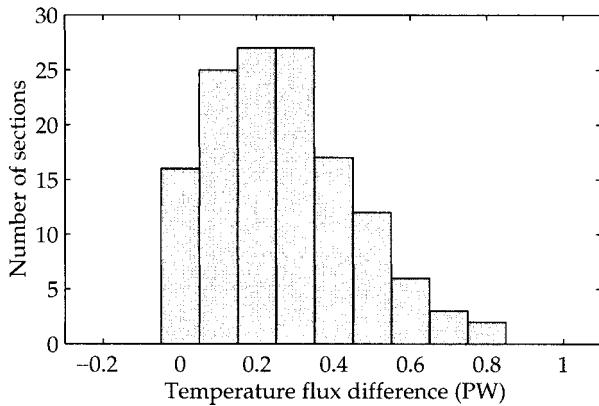

FIG. 11. Temperature flux difference in the Gulf Stream, between before use and after use of the parametric model, as a function of the number of sections.

on both sides of the basin, is 22 ± 8 Sv to the north, with a peak to peak range of 5 ± 3 Sv and a maximum in late summer. Analogously, the total baroclinic temperature flux of the upper layer is 1.4 ± 0.3 PW with an annual range of 0.6 ± 0.1 PW.

4) The zero net mass flux across the transect can be accomplished by assuming that below 2000 dbar an equivalent amount of water to that estimated for the upper layer flows in the southward direction. By assumption, most deep southward flow is concentrated in the deep western boundary current, with a potential temperature of 2.3°C. The temperature flux of the deep layer has an annual mean of -0.20 ± 0.06 PW and a peak to peak range of 0.05 ± 0.02 PW.

5) The total oceanic heat flux is estimated by adding the temperature fluxes of the upper and deep layers. The annual mean of the meridional heat flux is 1.2 ± 0.3 PW and the annual cycle has a range of 0.6 ± 0.1 PW.

6) Comparison with previous studies of the meridional heat flux at various locations in the North Atlantic shows similar results supporting our method of combining sections from different sectors. The value of

using historical hydrographic sections is that they span the widest range of time possible. Although the sections are not complete, they can be used to investigate temporal variability and to estimate the uncertainty involved in the heat flux calculations.

7) Although there are some indications of low-frequency change in the volume transport and heat flux, the short-term variability renders it difficult to obtain long-term means without considerable averaging, hence the grouping of data into pentadal periods. But even after doing this, only a few periods have enough sections for estimating changes in meridional heat flux. Significantly, for the three periods considered, in the late 1930s and in the 1970s, the heat fluxes appear to be the same within about 0.1 PW.

8) An important conclusion resulting from this study is that the smallness of low-frequency change is such that future studies must include a greater number of sections to reduce the contribution from the local eddy variability around the Gulf Stream and include explicitly the interannual changes in Ekman transport, which was beyond the scope of this study.

Future estimates might effectively be done from repeat acoustic Doppler current profiler sections across the ocean (preferably from merchant marine vessels) together with deep XBTs for temperature. Direct measurements of velocity and temperature to high spatial resolution (including the eddy field) will provide for much higher accuracies than present methods permit.

APPENDIX A

Ekman Temperature Flux

The temperature flux in the Ekman layer is

$$H_{EK} = C_p \int_0^L \frac{\tau_x}{f} \theta_{EK} \, dx. \quad (A1)$$

In practice, this integral is estimated zonally for every 1° of longitude by the product of the Ekman transport obtained from a climatological dataset to a mean temperature profile $\overline{\theta}_{EK}$.

The mean temperature within the Ekman layer was obtained from a weighted average using the meridional velocities profiles as weights. The meridional Ekman velocity profile $v(z)$ is given by Kundu (1990):

$$v(z) = \frac{-\tau_x/\rho}{\sqrt{f\nu}} e^{z/\delta} \sin\left(\frac{-z}{\delta} + \frac{\pi}{4}\right), \quad (A2)$$

where τ_x is the zonal component of the wind stress, ρ is the seawater density, f is the Coriolis parameter, ν is the eddy viscosity coefficient, and δ is the depth of the Ekman layer. As $v(z)$ will be used as weights, only the functional form v_n is relevant to this problem:

$$v_n(z) = e^{z/\delta} \sin\left(\frac{-z}{\delta} + \frac{\pi}{4}\right). \quad (A3)$$

Using the standard depths $z = (0, -10, -20, -30, -50, -75, -100$ m) and assuming an Ekman layer of constant depth of $\delta = -100$ m, and normalizing v_n to make the sum of the weights equal to one, results in a set of seven coefficients: $v_n(0) = 0.2263$, $v_n(-10) = 0.2184$, $v_n(-20) = 0.1988$, $v_n(-30) = 0.1726$, $v_n(-50) = 0.1150$, $v_n(-75) = 0.0539$, and $v_n(-100) = 0.0151$. The average velocity-weighted temperatures at each longitude x are obtained from

$$\overline{\theta}(x) = \sum_{z=0}^{-100} v_n(z)\theta(x, z). \quad (A4)$$

The product of the average velocity-weighted temperatures with the meridional Ekman transport obtained from the Bunker climatology is integrated longitudinally between the U.S. coastline and Europe to yield an estimate of the meridional heat transport due to Ekman transport.

APPENDIX B

Error Analysis

According to Eq. (3) the total meridional heat flux across a latitude is

$$H = H_{SW} + H_{GS} + H_{SS} + H_{MO} + H_{EK} + H_{DL}. \quad (B1)$$

For the error analysis a temperature representative of each sector is assumed to be a velocity-weighted temperature, which can be obtained dividing the temperature flux by the volume transport. Similarly, the volume transport representative of the sector is the annual mean volume transport. Then, the equation above can be rewritten as

$$H = \rho C_p [\overline{\theta}_{SW} \overline{V}_{SW} + \overline{\theta}_{GS} \overline{V}_{GS} + \overline{\theta}_{SS} \overline{V}_{SS} + \overline{\theta}_{MO} \overline{V}_{MO}$$

$$+ \overline{\theta}_{DL} \overline{V}_{DL}] + \frac{C_p \tau_x}{f} \Delta x \overline{\theta}_{EK}. \quad (B2)$$

TABLE B1. Mean and standard deviation in the temperature difference (°C) and volume transport (Sv) for each sector.

Region	$\overline{\theta}_i - \overline{\theta}_{DL}$	$\sigma_{\overline{\theta}_i - \overline{\theta}_{DL}}$	$\overline{V}_i$	$\sigma_{\overline{V}_i}$
SW	6.6	0.3	3	0.5
GS	12.6	0.05	69	1
SS	13.4	0.1	14	1
MO	12.9	0.5	34	2

To estimate the temperature flux of the deep layer, the volume transport conservation condition across the basin was used:

$$V_{SW} + V_{GS} + V_{SS} + V_{MO} + V_{DL} = 0. \quad (B3)$$

The transport V_{DL} from Eq. (B3) is substitute into Eq. (B2), which is rewritten in an index format:

$$H = \rho C_p \sum_{i=1}^{4} [(\overline{\theta}_i - \overline{\theta}_{DL})\overline{V}_i] + \frac{C_p \tau_x}{f} \Delta x \overline{\theta}_{EK}. \quad (B4)$$

a. Error of the baroclinic and barotropic components

The first four terms of Eq. (B4) contain the baroclinic and barotropic contribution of the heat flux. The standard deviation of the meridional heat flux is

$$\sigma_{H_B}^2 = \sigma_{\rho C_p}^2 \sum_{i=1}^{4} [(\overline{\theta}_i - \overline{\theta}_{DL})\overline{V}_i]^2 + \sigma_{(\overline{\theta}_i - \overline{\theta}_{DL})}^2 \sum_{i=1}^{4} [\rho C_p \overline{V}_i]^2$$

$$+ \sigma_{\overline{V}_i}^2 \sum_{i=1}^{4} [\rho C_p (\overline{\theta}_i - \overline{\theta}_{DL})]^2. \quad (B5)$$

The product ρC_p was assumed to be constant with depth and longitude. To estimate the error due to this assumption this product was calculated for all data. Its horizontal variability is very small and its standard deviation, mostly due to its vertical variation, is less than 0.002% throughout the region. The standard deviation of the heat due to ρC_p is 1.1×10^{11} W or 0.0001 PW, which is negligible. Table B1 shows a summary of the values used on the error estimation, which were determined directly from the dataset.

The error due to the uncertainties in the temperature is 0.09 PW and in the transport is 0.2 PW. Most of the uncertainties come from the transport, which is a derived quantity. The standard deviation in the baroclinic and barotropic components is 0.22 PW.

b. Error of the Ekman component

The variance in the estimation of the Ekman heat flux is

$$\sigma_{H_{EK}}^2 = \left(\frac{C_p \Delta x}{f}\right)^2 [(\sigma_{\overline{\tau}_x} \overline{\theta}_{EK})^2 + (\sigma_{\overline{\theta}} \overline{\tau}_x)^2]. \quad (B6)$$

The mean zonal component of the wind stress was estimated for latitude 36°N directly from the dataset, and it is found to be 0.07 N m^{-2}; a measurement error

of 20% was assumed. The temperature in the Ekman layer is a mean velocity-weighted temperature as described in Eq. (A4). The mean temperature within the Ekman layer was found to be 20.6°C, and a 10% of measurement error was assumed for standard deviation. The standard deviation error of the Ekman heat is 0.07 PW.

The estimation of the standard deviation in a root-mean-square sense yielded an overall error of the heat flux of 0.3 PW.

REFERENCES

Armi, L., and N. A. Bray, 1982: A standard analytic curve of potential temperature versus salinity for the Western North Atlantic. *J. Phys. Oceanogr.,* **12,** 384–387.

Bennett, A. F., 1978: Poleward heat fluxes in the Southern Hemisphere oceans. *J. Phys. Oceanogr.,* **8,** 785–798.

Bower, A. S., and T. Rossby, 1989: Evidence of cross-frontal exchange processes in the Gulf Stream based on isopycnal RAFOS float data. *J. Phys. Oceanogr.,* **19,** 1177–1190.

Bryan, K., 1962: Measurements of meridional heat transport by ocean currents. *J. Geophys. Res.,* **67,** 3403–3414.

Bunker, A. F., 1976: Computations of surface energy flux and annual air–sea interaction cycles of the North Atlantic Ocean. *Mon. Wea. Rev.,* **104,** 1122–1140.

Coachman, L. K., K. Aagaard, and R. B. Tripp, 1975: *Bering Strait: The Regional Physical Oceanography.* University of Washington Press, 172 pp.

Ezer, T., G. L. Mellor, and R. J. Greatbatch, 1995: On the interpentadal variability of the North Atlantic Ocean: Model simulated changes in transport, meridional heat flux and coastal sea level between 1955–1959 and 1970–1974. *J. Geophys. Res.,* **100,** 10 559–10 566.

Fillenbaum, E. R., T. L. Lee, W. E. Johns, and R. Zantopp, 1997: Meridional heat transport variability at 26.5°N in the North Atlantic. *J. Phys. Oceanogr.,* **27,** 153–174.

Greatbatch, R. J., A. F. Fanning, A. D. Goulding, and S. Levitus, 1991: A diagnosis of interpentadal circulation changes in the North Atlantic. *J. Geophys. Res.,* **96,** 22 009–22 023.

Halkin, D., and T. Rossby, 1985: The structure and transport of the Gulf Stream at 73°W. *J. Phys. Oceanogr.,* **15,** 1439–1452.

Hall, M. M., 1994: Synthesizing the Gulf Stream thermal structure from XBT data. *J. Phys. Oceanogr.,* **24,** 2278–2287.

——, and H. L. Bryden, 1982: Direct estimates and mechanisms of ocean heat transport. *Deep-Sea Res.,* **29,** 339–359.

Hastenrath, S., 1980: Heat budget of tropical ocean and atmosphere. *J. Phys. Oceanogr.,* **10,** 159–170.

Hendry, R. M., 1988: A simple model of the Gulf Stream thermal structure with application to analysis of moored measurements in the presence of mooring motion. *J. Atmos. Oceanic Technol.,* **5,** 328–339.

Hogg, N. G., 1986: On the correction of temperature and velocity time series for mooring motion. *J. Atmos. Oceanic Technol.,* **3,** 204–214.

——, 1991: Mooring motion corrections revisited. *J. Atmos. Oceanic Technol.,* **8,** 289–295.

Hsiung, J., 1985: Estimates of global oceanic meridional heat transport. *J. Phys. Oceanogr.,* **15,** 1405–1413.

Isemer, H.-J., and L. Hasse, 1987: *The Bunker Climate Atlas of the North Atlantic Ocean.* Vol. 2. *Air–Sea Interactions.* Springer-Verlag, 252 pp.

Johns, E., D. Watts, and H. Rossby, 1989: A test of geostrophy in the Gulf Stream. *J. Geophys. Res.,* **94,** 3211–3222.

Kundu, P. K., 1990: *Fluid Mechanics.* Academic Press, 638 pp.

Lamb, P. J., 1981: Estimate of annual variation of the Atlantic Ocean heat transport. *Nature,* **290,** 766–768.

Levitus, S., 1982: *Climatological Atlas of the World Ocean.* NOAA Prof. Paper No. 13, U.S. Govt. Printing Office, 173 pp.

——, and T. P. Boyer, 1994: *World Ocean Atlas 1994.* Vol. 4: *Temperature,* National Oceanographic Data Center, Ocean Climate Laboratory, 129 pp.

Luyten, J. R., 1977: Scales of motion in the deep Gulf Stream and across the Continental Rise. *J. Mar. Res.,* **35**(1), 49–73.

Mellor, G. L., C. R. Mechoso, and E. Keto, 1982: A diagnostic model of the general circulation of the Atlantic Ocean. *Deep-Sea Res.,* **29,** 1171–1192.

Molinari, R. L., E. Johns, and J. F. Festa, 1990: The annual cycle of meridional heat flux in the Atlantic Ocean at 26.5°N. *J. Phys. Oceanogr.,* **20,** 476–482.

Montgomery, R. B., 1974: Comments on ''Seasonal variability of the Florida current,'' by Niiler and Richardson. *J. Mar. Res.,* **32,** 533–535.

Oort, A. H., and T. H. VonderHaar, 1976: On the observed annual cycle in the ocean–atmosphere heat balance over the Northern Hemisphere. *J. Phys. Oceanogr.,* **6,** 781–800.

Pickart, R. S., and D. R. Watts, 1990: Deep western boundary current variability at Cape Hatteras. *J. Mar. Res.,* **48,** 765–791.

Rago, T. A., and H. T. Rossby, 1987: Heat transport into the North Atlantic Ocean north of 32°N latitude. *J. Phys. Oceanogr.,* **17,** 854–871.

Roemmich, D., 1980: Estimation of meridional heat flux in the North Atlantic by inverse method. *J. Phys. Oceanogr.,* **10,** 1972–1983.

——, and C. Wunsch, 1985: Two transatlantic sections: Meridional circulation and heat flux in the subtropical North Atlantic Ocean. *Deep-Sea Res.,* **32,** 619–664.

Sato, O. T., 1997: Seasonal and low frequency variability in the meridional heat flux at 36°N in the North Atlantic. Ph.D. thesis, Graduate School of Oceanography, University of Rhode Island, 148 pp.

——, and T. Rossby, 1995: Seasonal and low frequency variations in dynamic height anomaly and transport of the Gulf Stream. *Deep-Sea Res.,* **42,** 149–164.

Wall, F. J., 1986: *Statistical Data Analysis Handbook.* McGraw Hill, 285 pp.

Worthington, L. V., 1976: *On the North Atlantic Circulation.* Johns Hopkins Oceanographic Studies, No. 6, John Hopkins University Press, 110 pp.